JGR Atmospheres

RESEARCH ARTICLE
10.1029/2025JD044257

Special Collection:
Years of the Maritime Continent

Role of Diurnal Cycle of Insolation on the MJO Propagation in the Maritime Continent

Xin Zhou[1,2], Pallav Ray[2], Jimy Dudhia[1], Samson Hagos[3], Nathaniel C. Johnson[4], Efthymios Nikolopoulos[5], and Bradford S. Barrett[6]

[1]National Center for Atmospheric Research (NCAR), Boulder, CO, USA, [2]Florida Institute of Technology, Melbourne, FL, USA, [3]Pacific Northwest National Laboratory (PNNL), Richland, WA, USA, [4]NOAA Geophysical Fluid Dynamics Laboratory (GFDL), Princeton, NJ, USA, [5]Civil and Environmental Engineering, Rutgers University, Piscataway, NJ, USA, [6]Independent Scholar, Raleigh, NC, USA

Abstract The diurnal cycle of convection in the Maritime Continent (MC) has been hypothesized to act as a barrier to the eastward propagation of the Madden-Julian oscillation (MJO). To test this hypothesis, we use a regional model with realistic MJO to simulate an event from the boreal spring of 2013 that weakened and stalled over the MC. Two simulations are conducted: one that includes the diurnal cycle of insolation (CTL), and another without it (NO_DC). The MJO in the simulations was identified and tracked using a large-scale precipitation tracking method that distinguishes propagation and non-propagation unlike the usual Real-time Multivariate MJO method. In the NO_DC simulation, the absence of diurnal heating reduces land precipitation, allowing more continuous eastward MJO propagation. An analysis of moist static energy budget reveals that MJO maintenance in NO_DC is due to increased longwave heating and reduced advection, whereas the persistent MJO propagation in NO_DC is due to increased advection and reduced longwave heating and surface latent heat flux. These processes, however, may vary across different parts of the MC, emphasizing the complexity of MJO propagation across the MC.

Plain Language Summary The Madden-Julian Oscillation (MJO) is a major large-scale weather system with a roughly 30–60-day cycle that influences tropical rainfall and global atmospheric circulation. As the MJO moves eastward across the Indo-Pacific Maritime Continent (MC), its strength often diminishes, making it difficult to predict. One possible reason for this weakening is the strong daily cycle of heating and cooling over the MC's islands, which creates land-sea breezes and localized thunderstorms. To investigate this, we used a high-resolution weather model to simulate an MJO event under two conditions: one with the natural daily solar radiation (CTL) and one without it (NO_DC). Our results show that when the daily heating cycle is removed, the land-sea breeze weakens and rainfall shifts from land to ocean, allowing the MJO to move more smoothly across the region. This suggests that the absence of daily heating reduces disruptions in the large-scale moisture and energy transport that drive MJO propagation. Our findings highlight the critical role of the daily solar radiation cycle in shaping tropical weather. Improving how weather models represent these processes could lead to more accurate forecasts of the MJO and its global impacts, including extreme weather events.

Key Points:

- The diurnal cycle of convection disrupts Madden-Julian oscillation (MJO) propagation by enhancing convection over land and weakening convection over ocean
- Robust MJO maintenance without the diurnal cycle of convection is due to increased longwave heating
- Persistent MJO propagation without the diurnal cycle of convection is primarily due to increased advection of moist static energy

Supporting Information:

Supporting Information may be found in the online version of this article.

Correspondence to:

S. Hagos,
Samson.Hagos@pnnl.gov

Citation:

Zhou, X., Ray, P., Dudhia, J., Hagos, S., Johnson, N. C., Nikolopoulos, E., & Barrett, B. S. (2025). Role of diurnal cycle of insolation on the MJO propagation in the maritime continent. *Journal of Geophysical Research: Atmospheres*, *130*, e2025JD044257. https://doi.org/10.1029/2025JD044257

Received 1 MAY 2025
Accepted 4 NOV 2025

Author Contributions:

Formal analysis: Xin Zhou
Funding acquisition: Pallav Ray
Methodology: Xin Zhou, Pallav Ray, Jimy Dudhia, Samson Hagos
Writing – original draft: Xin Zhou, Pallav Ray

1. Introduction

The Indo-Pacific Maritime Continent (MC) is a geographically complex region characterized by numerous islands and enclosed seas along the equator (Ramage, 1968). Surrounded by warm sea surface temperatures (SSTs), the MC experiences pronounced deep convection that is amplified over land, particularly over elevated terrain (Abhik, Hendon, & Zhang, 2023, Abhik, Zhang, & Hendon, 2023; Hagos et al., 2016; Kerns & Chen, 2016; D. Kim et al., 2020; Rui & Wang, 1990; Salby & Hendon, 1994; Tan et al., 2022; Zhang & Ling, 2017). This enhanced convection over the larger islands often disrupts the Madden-Julian oscillation (MJO; Madden & Julian, 1971), the dominant mode of sub-seasonal atmospheric variability in the tropics, leading to its weakening or stalling as it propagates through the MC (e.g., Bai & Schumacher, 2022; Hsu & Lee, 2005; Ling et al., 2019; Pohl & Matthews, 2007; Tan et al., 2020; Yadav & Straus, 2017; Zhang & Hendon, 1997). Despite its importance, MJO propagation through the MC remains poorly represented in many numerical models (Jiang et al., 2020; D. Kim et al., 2009; H. M. Kim et al., 2016), posing significant challenges to its skillful prediction (Ahn et al., 2020; Ray et al., 2011; Seo et al., 2009; Vitart & Molteni, 2010; Wang et al., 2019; X. Zhou et al., 2024). However, recent studies suggest that this forecast barrier is not an intrinsic limitation to the MJO but

Writing – review & editing: Xin Zhou, Pallav Ray, Jimy Dudhia, Samson Hagos, Nathaniel C. Johnson, Efthymios Nikolopoulos, Bradford S. Barrett

can be mitigated with improved understanding of key physical processes and their representations in models (e.g., H. Kim et al., 2021; Neena et al., 2014).

One potential contributor to the MJO prediction barrier in the MC is its interaction with the region's pronounced diurnal cycle of convection (Abhik, Hendon, & Zhang, 2023, Abhik, Zhang, & Hendon, 2023; Li et al., 2020). Forced by strong land-sea breeze circulations, the diurnal cycle drives significant convection and precipitation, especially over larger islands like Sumatra, Borneo, and New Guinea (Ichikawa & Yasunari, 2006, 2008; Tan et al., 2021; Yang & Slingo, 2001; Y. Zhou et al., 2022, 2023). While the diurnal cycle plays a crucial role in shaping the tropical climate and its variability (Houze et al., 1981; Love et al., 2011; Lu et al., 2019; Mori et al., 2004; Rauniyar & Walsh, 2011; Yamanaka, 2016), its influence on MJO propagation remains elusive as some MJO events are weakened over the MC, while others propagate across the MC unaffected (e.g., Barrett et al., 2021; Peatman et al., 2014; Rauniyar & Walsh, 2011; Tian et al., 2006; Wei et al., 2020).

Some studies suggest that strong diurnal convection over land may interfere with MJO convection over adjacent oceanic regions, weakening its signal (Sobel et al., 2010; Zhang & Ling, 2017). Numerical simulations have shown that reducing the amplitude of the diurnal cycle of convection over land can enhance MJO propagation (Hagos et al., 2016; Oh et al., 2013; Wei et al., 2020), possibly through moist entropy advection (Jiang, 2017) associated with the moisture mode framework (Jiang et al., 2020) of the MJO. Furthermore, shading effects from cirrus clouds ahead of the propagating MJO may lead to SST cooling, thereby reducing available moist static energy (MSE) (Karlowska et al., 2024; Matthews, 2000; Suzuki, 2009; Tian et al., 2006). However, while these processes occur on the sub-seasonal time scale, the physical mechanisms through which the diurnal cycle of insolation affects MJO propagation across the MC remain unclear.

Moreover, while extended-range and seasonal forecast models do include the diurnal cycle of insolation, many of these models still struggle to capture the eastward propagation of the MJO through the MC (Jiang et al., 2020; D. Kim et al., 2009; H. M. Kim et al., 2016). This indicates that the challenge lies not in the absence of the diurnal cycle per se, but in how diurnally-forced land–sea contrasts and related diurnal convection interact with the large-scale evolution of MJO convection. To address this gap, we investigate the impact of the diurnal cycle of insolation on MJO amplitude and propagation in the MC using regional model simulations. Unlike conventional MJO tracking methods that rely on the Real-time Multivariate MJO (RMM) index (Wheeler & Hendon, 2004), we use a recently-developed tracking approach to distinguish propagating from non-propagating MJO events. Additionally, we conduct a budget analysis of MSE to explore the physical mechanisms through which the diurnal cycle influences the simulated MJO amplitude and propagation. The rest of the paper is organized as follows: Section 2 describes the model, data, and methods, followed by the results in Section 3 and conclusions in Section 4.

2. Methods, Model, and Data

2.1. Model and Data

To investigate the role of the diurnal cycle on the MJO, two simulations were conducted using version 4.4 of the Weather Research and Forecasting (WRF) model with the Advanced Research WRF dynamic core (Powers et al., 2017). The first simulation, referred to as the control (CTL) simulation, included the natural diurnal cycle of incoming solar radiation at the top of the atmosphere (TOA). The second simulation, a sensitivity experiment (NO_DC), maintained a constant daily mean solar flux (Figure 1b). The model domain extends from 20°S to 20°N and from 87°E to 158°E (Figure 1a), with most analyses focused on the 10°S to 10°N region. In our experiments, the diurnal cycle of insolation was removed across the full model domain (20°S–20°N, 87°E–158°E), ensuring that the treatment is not sensitive to the choice of a specific sub-domain. Both simulations were performed with a 10 km grid spacing and 43 vertical levels. The 10 km grid spacing allows the WRF simulations to explicitly resolve mesoscale land–sea breeze circulations and their associated diurnal cycle of convection, consistent with previous studies of the MC (e.g., Ling et al., 2019; Love et al., 2011; Y. Zhou et al., 2022). Initial and boundary conditions were obtained from the ECMWF Reanalysis v5 (ERA5) data set (Hersbach et al., 2020). Further details on model configurations and physics parameterizations are provided in Table 1. The simulations covered 1–31 May 2013, with output recorded every 3 hr. We selected May 2013 because it featured a well-documented MJO event that propagated into the MC and subsequently weakened, providing a clear case to examine the barrier effect of the diurnal cycle. This event has also been studied in prior work (Ling et al., 2019; Ren et al., 2021), reinforcing its relevance for sensitivity experiments. Moreover, this period is characterized by neutral ENSO, thereby minimizing the influence of interannual variability and allowing us to isolate more directly the role of the

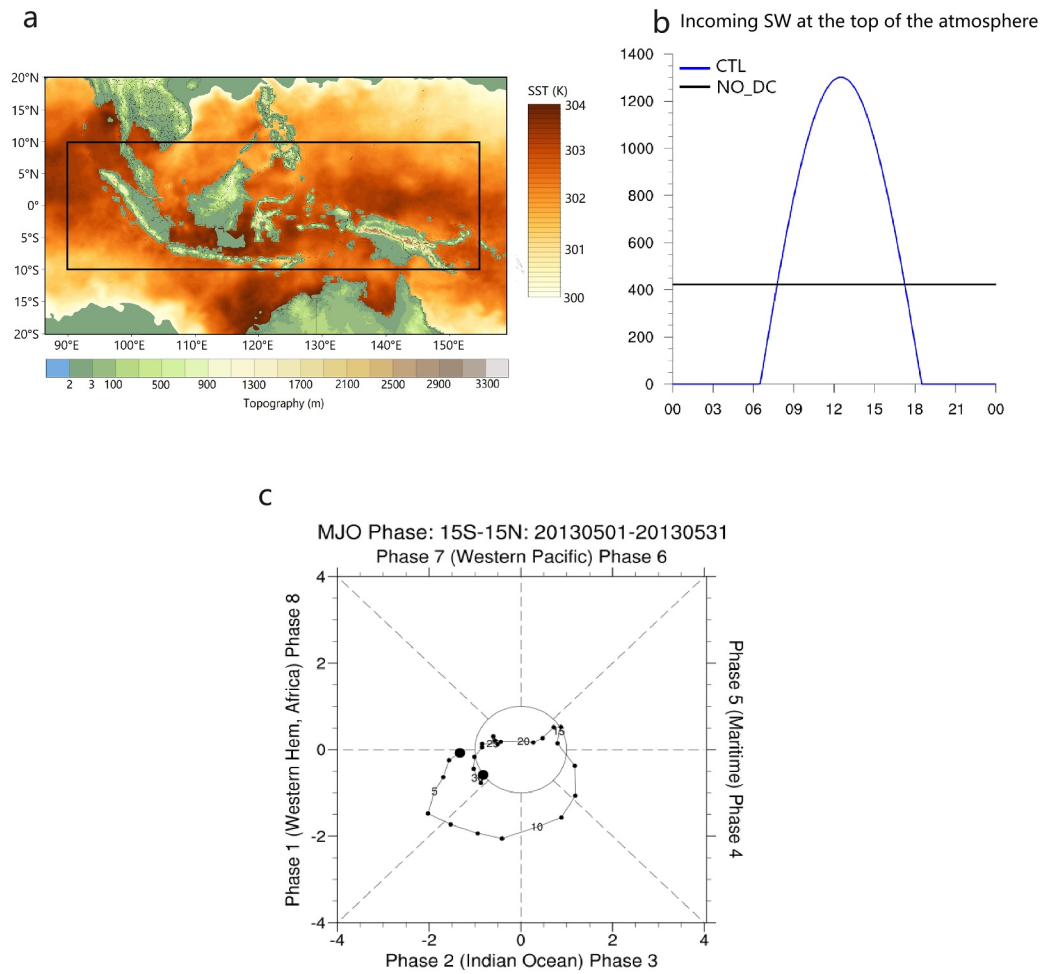

Figure 1. (a) Model domain (87°E–158°E, 20°S–20°N) and the primary focus area (black rectangle, 90°E–155°E, 10°S–10°N) along with topographic height (m, shaded) and sea surface temperature (K, shaded) for May 2013. (b) Top of the atmosphere downwelling shortwave radiation (W m^{-2}) from the CTL and NO_DC simulations averaged over the simulation period (1–31 May 2013). (c) Madden-Julian oscillation (MJO) propagation from 1 May 2013 to 31 May 2013 as represented in the phase space based on the Real-Time MJO Multivariate (RMM) index of Wheeler and Hendon (2004).

Table 1
Summary of Model (WRF) Configurations

Model (WRFv4.4) specifications and parameterizations		Reference
Horizontal resolution	10 km	
Vertical layers	43	
Temporal resolution	3 hourly	
Model top	10 hPa	
Microphysics	WRF Single Moment 6 (WSM6) scheme	Lim and& Hong (2010)
Cumulus parameterization	modified Tiedtke scheme	Tiedtke (1989)
Surface layer parameterization	Noah land surface model scheme	Chen and& Dudhia (2001)
Longwave and shortwave radiation	Rapid Radiative Transfer Model for GCMs (RRTMG) schemes	Iacono et al. (2008)
Planetary boundary layer	Yonsei University (YSU) Scheme	Hong and Lim. (2006)
Initial and boundary conditions	ERA5 reanalysis	Hersbach et al. (2020)

diurnal cycle in MJO propagation. While we acknowledge that SST biases could influence the background state, our conclusions are based on a relative comparison between CTL and NO_DC simulations, both driven by identical ERA5 forcing. This design minimizes the impact of potential absolute SST biases on the key results of this study.

To analyze precipitation characteristics, we use satellite observations from the Tropical Rainfall Measuring Mission (TRMM, Liu et al., 2012). TRMM was a joint mission between NASA and JAXA designed to monitor tropical and subtropical rainfall and improve our understanding of the global water and energy cycle. In this study, we use the TRMM 3B42 version 7 product, which provides 3-hourly precipitation estimates on a 0.25° × 0.25° latitude–longitude grid. The 3B42 algorithm combines information from TRMM's Precipitation Radar, the TRMM Microwave Imager (TMI), and other passive microwave sensors, and calibrates them against rain gauge observations to reduce bias. This data set has been widely used for studies of tropical precipitation variability, diurnal cycle, extreme rainfall, and hydrological applications.

2.2. Methods

2.2.1. Large-Scale Precipitation Tracking (LPT)

We used the large-scale precipitation tracking (LPT, Kerns & Chen, 2016, 2020) method to identify MJO events and track their propagation. We chose LPT because it identifies coherent precipitation systems and distinguishes between propagating and non-propagating events, in contrast to the traditional RMM index, which often cannot differentiate stalled convection from eastward-moving disturbances (Kiladis et al., 2014). The LPT method has been successfully applied in prior MJO studies (Kerns & Chen, 2016; Savarin & Chen, 2023) and has been shown to robustly capture the spatial and temporal characteristics of MJO-related precipitation. While no single tracking metric is without limitations, LPT provides a more direct precipitation-based framework that aligns with the objectives of our study.

The LPT method identifies large-scale precipitation features using a threshold for 3-day accumulated rainfall rate. For this study, we set the threshold at 10 mm day$^{-1,}$ based on tests with thresholds ranging from 5 to 15 mm day^{-1}. Lower thresholds tended to merge extensive areas of warm pool precipitation into a single feature, whereas higher thresholds resulted in fragmented, shorter tracks — neither of which is characteristic of the MJO. Only precipitation features with a minimum size of 400 grid points (approximately 4×10^4 km^2, or 200 km × 200 km) were considered. Additionally, the centroids of these precipitating features had to be within 15°S–15°N latitude. Precipitation features were identified every three hours from model outputs from 01 May 2013 to 31 May 2013, providing a detailed temporal resolution for tracking the evolution and movement of these features. This approach allows us to effectively monitor the progression and characteristics of MJO-related precipitation across the MC.

2.2.2. Column-Integrated Moist Static Energy (MSE) Budget

The MSE is defined as the sum of dry static energy (DSE) and latent energy (LE), and is given by:

$$\mathrm{MSE} = C_p T + gz + L_v q \tag{1}$$

$$\mathrm{DSE} = C_p T + gz \tag{2}$$

$$\mathrm{LE} = L_v q \tag{3}$$

where T is the air temperature, C_p is the specific heat at constant pressure, z is the height, g is the gravitational acceleration, q is the specific humidity, and L_v is the latent heat of condensation.

The column-integrated MSE budget in pressure coordinates is given by (e.g., Ren et al., 2021):

$$<\frac{\partial \mathrm{MSE}}{\partial t}>' = -<V_h \cdot \nabla \mathrm{MSE}>' - <\omega \frac{\partial \mathrm{MSE}}{\partial p}>' + \mathrm{LH}' + \mathrm{SH}' + <\mathrm{LW}>' + <\mathrm{SW}>' + R \tag{4}$$

where $< >$ indicates a mass-weighted vertical integral from the surface to 100 hPa, and the prime indicates anomalies. V_h is the horizontal wind, ω is the vertical velocity, p is the pressure, LH and SH denote latent and

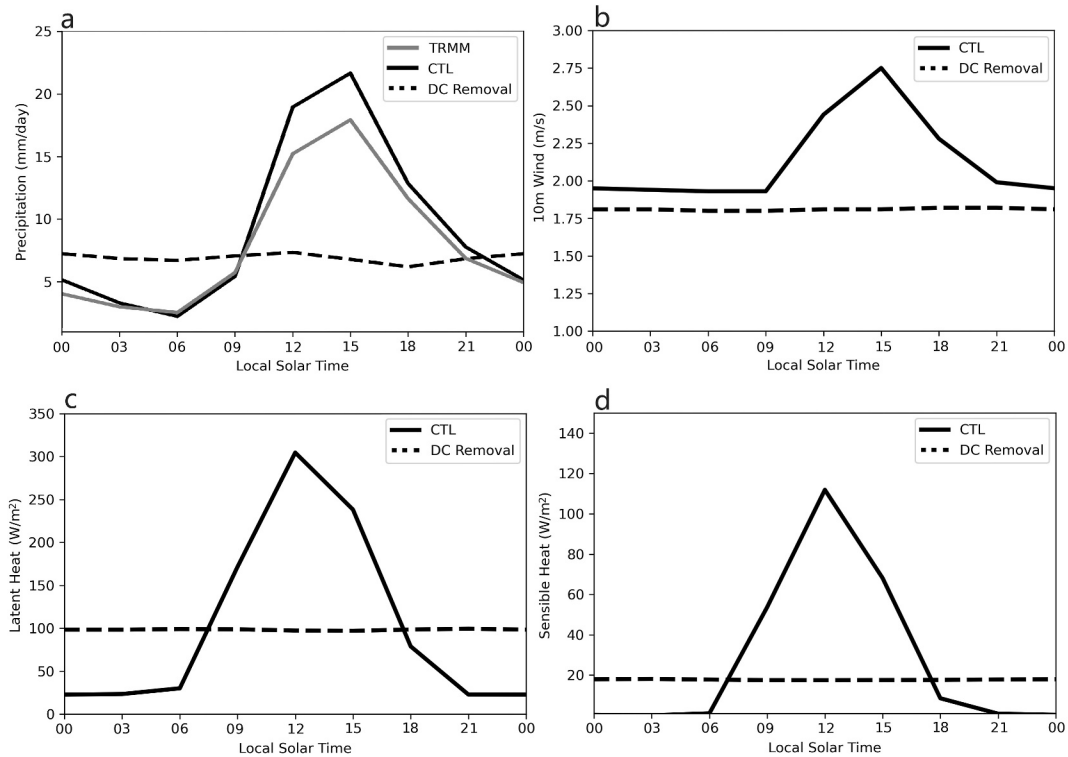

Figure 2. The diurnal cycle of (a) mean rain rate (mm day^{-1}), (b) 10 m winds (m s^{-1}), (c) surface latent heat flux (W m^{-2}), and (d) surface sensible heat flux (W m^{-2}) averaged over the islands from Tropical Rainfall Measuring Mission (solid gray line), CTL (solid black lines) and NO_DC (dashed black lines) simulations during 01–31 May 2013.

sensible heat flux at the surface, respectively, and LW and SW represent the column-integrated longwave and shortwave radiative heating rates. The residual is denoted by R. Equation 4 shows the local tendency of MSE on the left, while the first two terms on the right-hand side represent horizontal advection (HADV) and vertical advection (VADV) of MSE.

To assess the contributions of individual budget terms to the maintenance and propagation of MSE anomalies, we project these terms onto the MSE anomalies and their tendencies, following Andersen and Kuang (2012). The contribution of a source x to the maintenance (m) and propagation (p) of the MJO is calculated as:

$$S_m(x) = \frac{||x'M'||}{||M'M'||} \tag{5}$$

$$S_p(x) = \frac{||x'(\partial M'/\partial t)||}{||(\partial M'/\partial t)(\partial M'/\partial t)||} \tag{6}$$

where $||A||$ is the integral of A over the domain considered, and x' and M' are MSE budget terms in Equation 4 and MSE column-integrated anomaly, respectively.

3. Results

3.1. Impact of the Diurnal Cycle of Insolation

The NO_DC simulation exhibits a noticeably weaker diurnal variation in precipitation, with reduced rainfall over land compared to the CTL simulation (Figure 2 and Table 2). This reduction is primarily due to a weaker convection over the land (Hagos et al., 2016). Additionally, the absence of a diurnal radiation cycle in NO_DC reduces variability in near-surface meteorological variables, such as winds and humidity, resulting in minimal variation in surface latent and sensible heat flux (Figures 2c and 2d). Overall, latent heat flux in the NO_DC

Table 2
Precipitation (mm Day^{-1}), Surface Skin Temperature (K), Surface Latent Heat Flux (W m^{-2}) and Surface Sensible Heat Flux (W m^{-2}) From CTL, NO_DC, and Their Difference (NO_DC Minus CTL) Over the Islands of the Maritime Continent for 01–31 May 2013

	CTL	NO_DC	NO_DC-CTL
Precipitation	11.2	7.7	−3.5 (−31.3%)
Surface temperature	299.3	300.5	1.2 (0.4%)
Latent heat	121.5	99.7	−21.8 (−17.9%)
Sensible heat	41.3	18.9	−22.4 (−54.2%)

simulation is reduced by 21.8 W m^{-2} (−17.9%), and sensible heat flux decreases by 22.4 W m^{-2} (−54.2%) compared to the CTL. This decline in surface latent heat flux is due to decreased precipitation and winds (Figures 2a and 2b), whereas the reduction in sensible heat flux is due to weaker near-surface winds (Figure 2b) and air-sea temperature contrast (not shown).

The effect of the diurnal cycle on MJO propagation is examined using the LPT method (Figure 3). In the CTL simulation (Figure 3a), the MJO dissipates around Sumatra, highlighting the barrier effect of the MC. In contrast, in the NO_DC simulation (Figure 3b), the MJO persists longer, advancing farther east with a propagation speed of ∼5.3 m s^{-1}. Figure 4 presents the composite of large-scale precipitation associated with the MJO following Kerns and Chen (2020), clearly showing the barrier effect in CTL and the successful MJO crossing in NO_DC. By 20 May 2013, the MJO reaches New Guinea, with its centroid progressing across the MC before dissipating near 135°E. These results indicate that removing the diurnal cycle allows the MJO to maintain its strength and propagate further across the MC compared to the CTL simulation. The causes behind this are explored next through an analysis of the MSE budget.

3.2. Mean Precipitation and Moist Static Energy

Figure 5 illustrates the horizontal distributions of the 10-day (10–20 May 2013) mean precipitation and column-integrated MSE, DSE, and LE (see Equations 1–3). In the CTL simulation (Figure 5a), precipitation is heavier over the islands and lighter over the ocean. In contrast, the NO_DC simulation (Figure 5b) shows the opposite pattern, with more precipitation over the ocean and less over the islands. The decline in precipitation over the islands (Figure 5c) is particularly pronounced over southwestern Borneo and New Guinea.

The MSE structures (Figures 5d and 5e) are primarily driven by the LE (Figures 5j and 5k), with a high pattern correlation coefficient (CC = 0.76), while the DSE (Figures 5g and 5h, CC = 0.39) remains relatively uniform. This is consistent with previous studies (Ren et al., 2021). As a result, the difference in MSE (Figure 5f) between the CTL and NO_DC simulations is mainly due to differences in LE (Figure 5l). In the oceanic regions surrounding the islands in the MC, MSE is higher in the NO_DC compared to the CTL (Figure 5f), resulting in enhanced oceanic precipitation that facilitates smoother MJO propagation across the MC, and is consistent with Ling et al. (2019).

Similar to the horizontal structure (Figure 5), the vertical structure of MSE differences (Figure 6a) aligns more closely with the LE differences (Figure 6c) (CC = 0.73) than with the DSE (Figure 6b) (CC = 0.39). Longitudinal variations in MSE in the mid-to lower troposphere are primarily driven by LE, particularly between 110°E and 130°E. In contrast, DSE differences (Figure 6b) remain relatively uniform along longitudes except in the

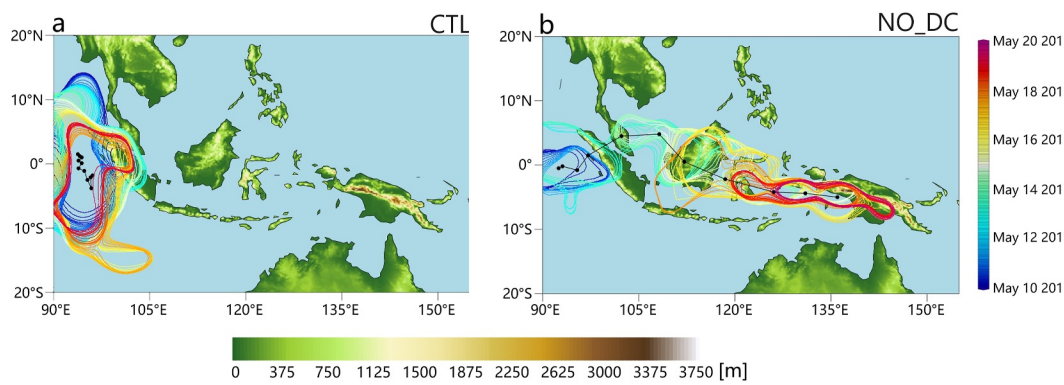

Figure 3. Topographic height (shaded, m) and spatiotemporal evolution of large-scale precipitation objects from the (a) CTL and (b) NO_DC simulations during 10–20 May 2013. Color shading of the contours represents time, with initial times depicted in navy blue and later times in magenta. The black line indicates the daily path of the centroid of large-scale precipitation objects. The average propagation speed of Madden-Julian oscillation for NO_DC based on panel b is about 5.3 m s^{-1} (4.1° day^{-1}).

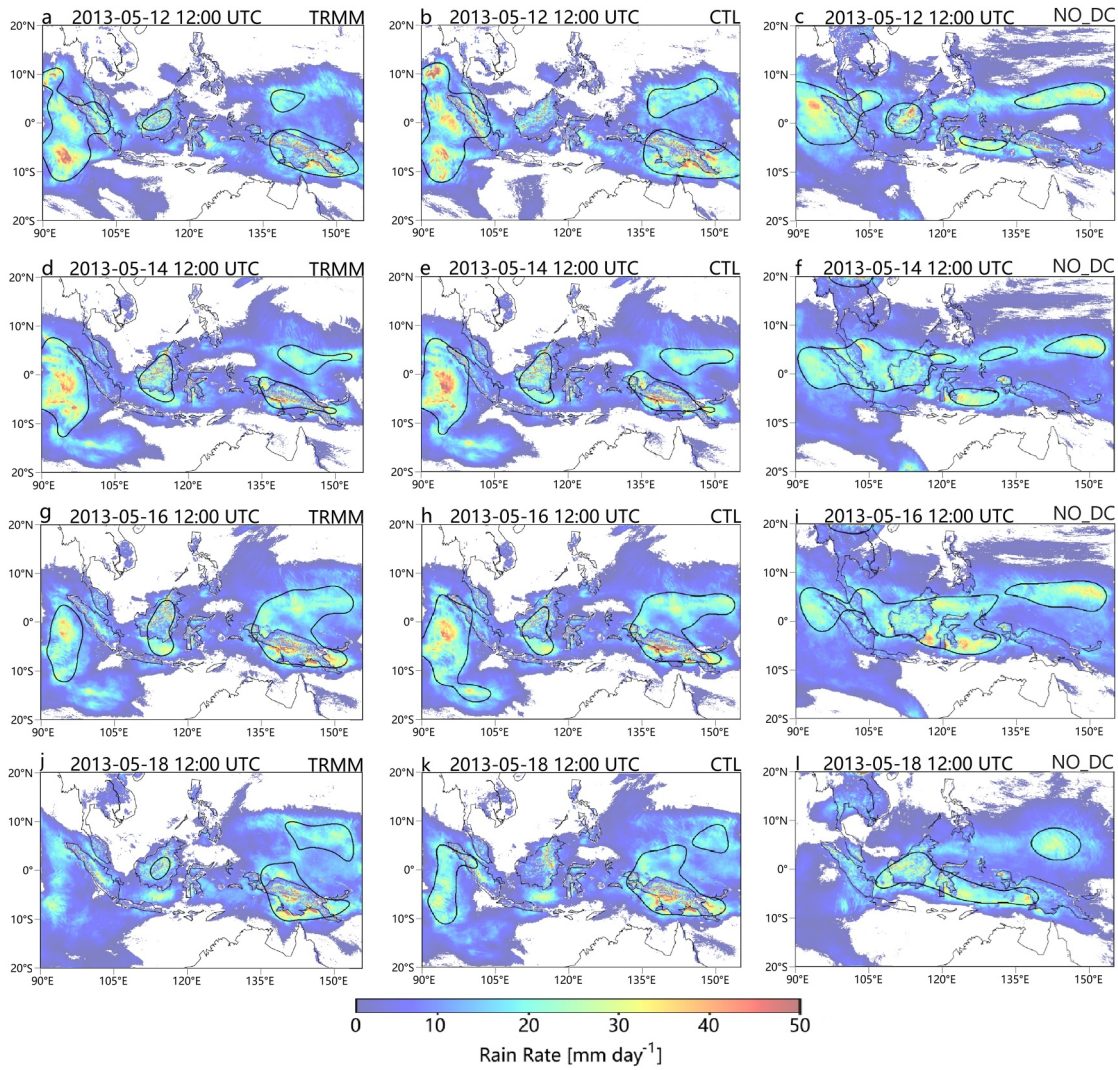

Figure 4. The Daily precipitation at representative stages of the Madden-Julian oscillation life cycle in large scale precipitation from the (left) Tropical Rainfall Measuring Mission, (middle) CTL and (right) NO_DC simulations for (a–c) 12 May 2013, (d–f) 14 May 2013, (g–i) 16 May 2013, and (j–l) 18 May 2013.

boundary layer and near 200 hPa. The area-averaged profiles of MSE differences (Figure 6d) are most pronounced around 950 hPa and 500 hPa. The CTL simulation shows higher MSE over land and lower MSE over the ocean compared to NO_DC (Figure 5). The diurnal radiation cycle amplifies daytime convection over land, which strongly influences vertical energy transport. Ocean-dominated regions (e.g., 120°E to 130°E) in the NO_DC simulation exhibit greater moisture and warmer temperatures in the lower layers of the troposphere (Figure 6d). This is because the absence of the diurnal cycle reduces convection over land, leading to stronger convection over the ocean, which efficiently ventilates heat and moisture from the planetary boundary layer (PBL) to higher altitudes (Figure 6d).

Conversely, in land-dominated regions, the NO_DC simulation shows lower MSE than the CTL, as the removal of the diurnal cycle weakens vertical mixing and convection, thereby limiting the ventilation of heat and moisture from the PBL. These differences highlight the importance of vertical mixing and deep convection in controlling heat and moisture distribution. The role of these differences in the horizontal and vertical structures of MSE between the CTL and NO_DC simulations on the maintenance and propagation of the MJO is explored next.

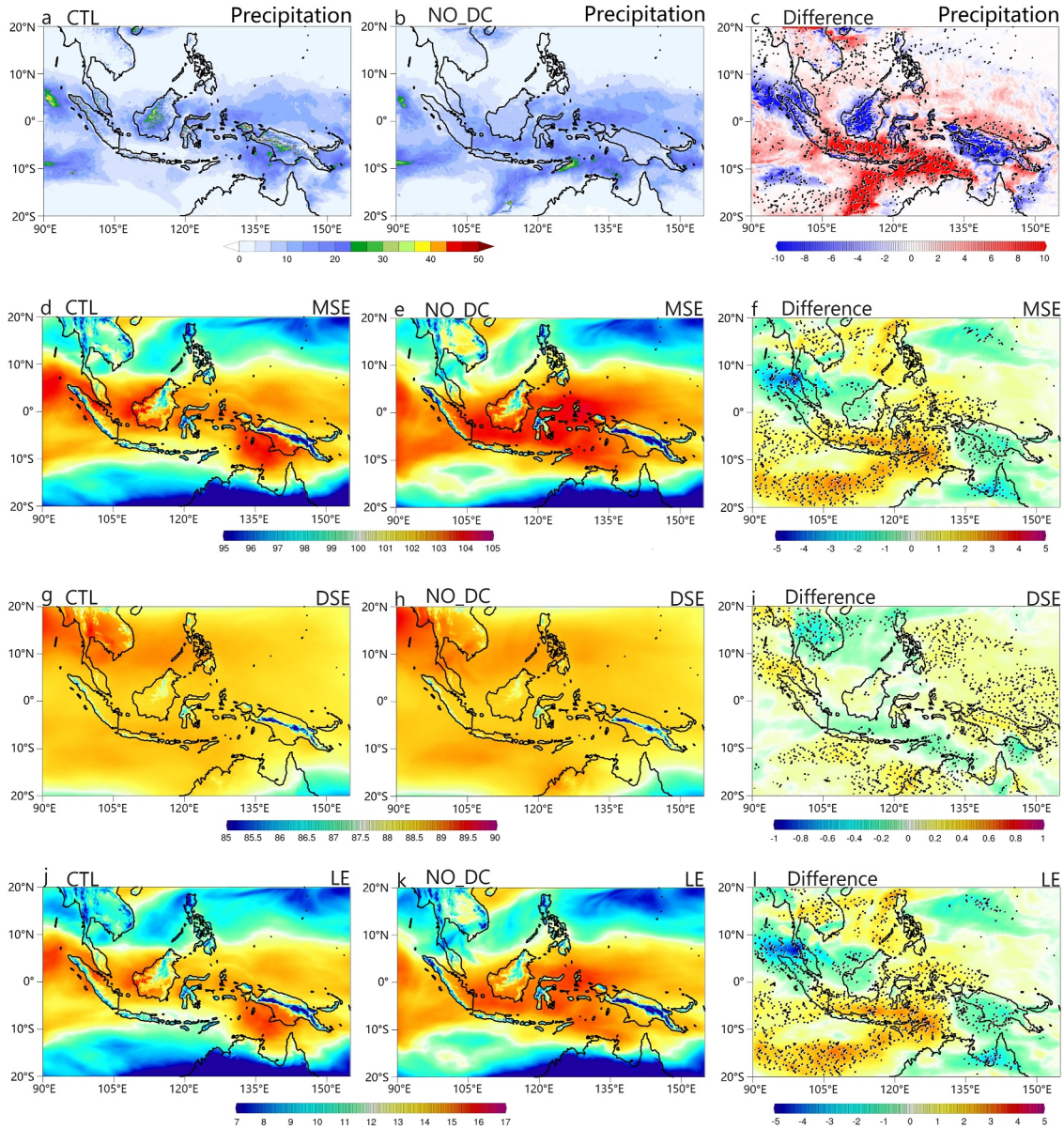

Figure 5. (Left panels) Mean (10–20 May 2013) (a) precipitation (mm day^{-1}), column-integrated (d) moist static energy (10^6 J kg^{-1}), (g) dry static energy (10^6 J kg^{-1}) and (j) latent energy (10^6 J kg^{-1}) from CTL over the Maritime Continent. Middle panels (b, e, h, k) are the same as the left panels but from NO_DC. Right panels (c, f, i, l) are the difference (NO_DC-CTL). Dotted areas in (c, f, i, l) indicate where the difference is statistically significant at the 95% level based on a student's *t*-test.

3.3. Maintenance and Propagation of the MJO

The differences in MSE closely align with the differences in LE below 200 hPa and with DSE above 200 hPa. The largest MSE difference occurs at 500 hPa, reaching 0.8 kJ kg^{-1}, with LE differences (0.66 kJ kg^{-1}) accounting for 82% of the total MSE difference in Figure 6d. This indicates that LE is the primary contributor to the MSE differences between the simulations, emphasizing its critical role in influencing the vertical structure of MSE.

To assess the contributions to the maintenance and propagation of MSE anomalies, we project anomalies in the budget terms onto the MSE anomaly and its time derivative (Equation 4). This allows us to identify the terms that most significantly contribute to the maintenance or dissipation of the anomaly (Equation 5), as well as those that help or hinder its propagation (Equation 6). Figure 7 (left panels) shows the fractional contributions to the maintenance of the MSE anomaly from each term in the MSE budget. The LW emerges as the dominant source of

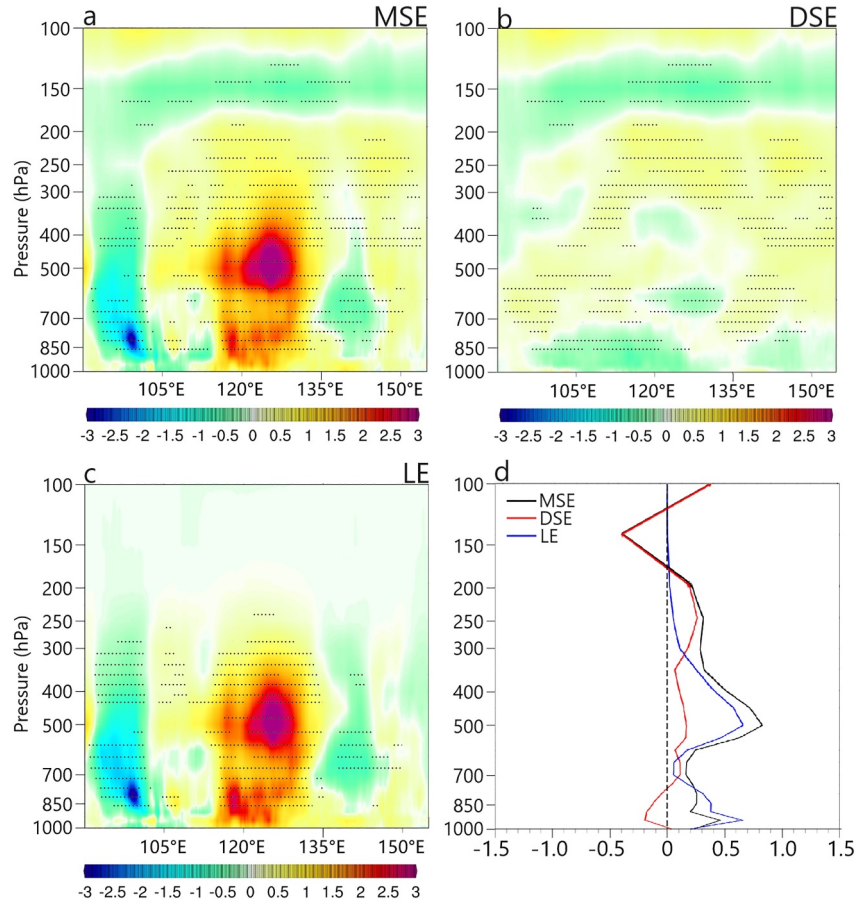

Figure 6. Longitude–pressure distribution of the differences between the CTL and NO_DC (NO_DC minus CTL) for (a) moist static energy (kJ kg^{-1}), (b) dry static energy (kJ kg^{-1}), and (c) latent energy (kJ kg^{-1}) averaged over 10°S–10°N during 10–20 May 2013. (d) Area averaged (10°S–10°N, 90°E–155°E) profiles based on (a), (b), and (c). Dotted areas in (a, b, c) indicate where the difference is statistically significant at the 5% level based on a Student's *t*-test.

column-integrated MSE for the MJO, followed by VADV, while SH has a minimal contribution. These findings largely agree with previous studies (Andersen & Kuang, 2012).

In maintaining the MJO MSE anomalies (Figures 7a, 7c, and 7e), VADV and LW are the primary contributors. For instance, in regions of enhanced MJO convection, MSE is exported out of the column via vertical MSE advection, while anomalous longwave radiation partially compensates for the MSE loss. In the NO_DC simulation, smaller contributions from HADV and VADV, coupled with larger contributions from LW, result in a reduced damping effect on MSE compared to the CTL simulation (Wolding et al., 2016). In contrast, SW and LH provide a non-negligible positive contribution to the MSE amplitude, consistent with findings from Ren et al. (2021). Because radiative heating, precipitation, and moisture are closely linked for MJO, cloud-radiative feedback acts as a destabilizing influence; however, it does not contribute to MJO propagation (Sobel & Maloney, 2013). The differences in these contributions between the NO_DC and CTL simulations are summarized in Table 3.

For the eastward propagation of MJO MSE anomalies (Figure 7, right panels), advection processes dominate, while LH and LW act to oppose this eastward movement (Andersen & Kuang, 2012; Ren et al., 2021). Among the advection terms, VADV plays a more dominant role in the propagation of MSE anomalies compared to HADV. In previous studies, HADV of MSE has been identified as a key process for recharge and discharge of moisture, which is critical for the eastward propagation (J. K. Kim & Sobel, 2014) or stalling (Wolding et al., 2016) of the MJO. In the NO_DC simulation, both horizontal and VADV terms are larger, indicating that they are significant sources of MSE that facilitate the eastward propagation of the MJO. This suggests that removing the diurnal cycle

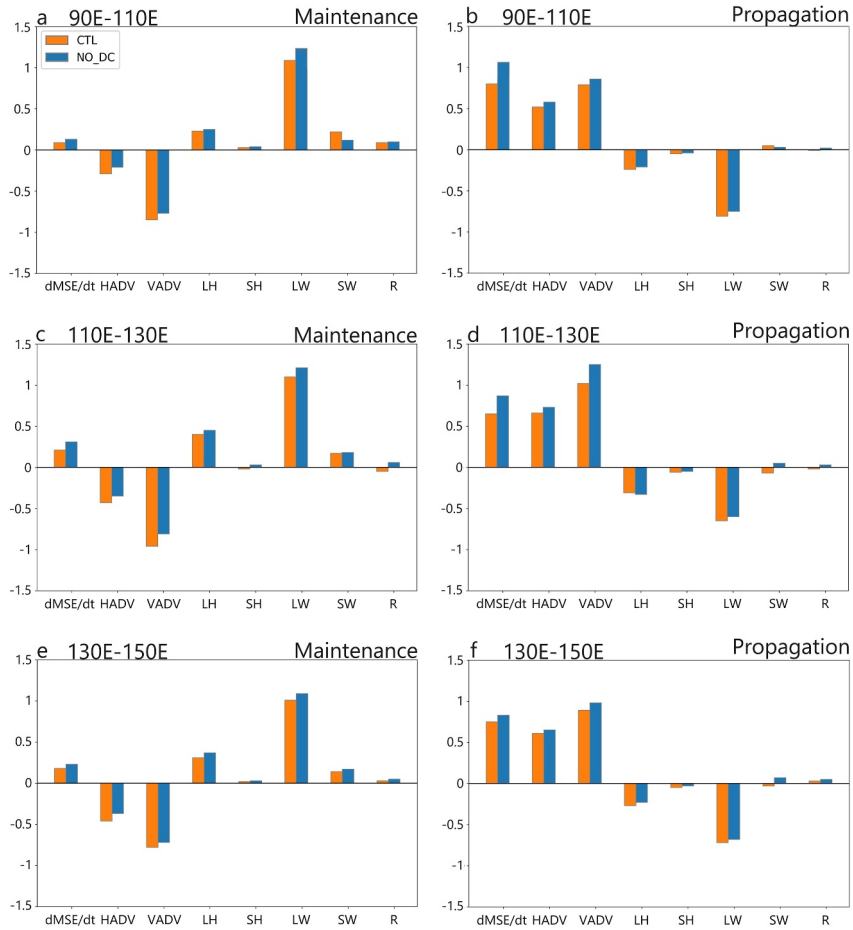

Figure 7. (Upper panel) Fractional contributions of the individual moist static energy (MSE) budget terms (no units) to the (a) maintenance, and (b) propagation of the Madden-Julian oscillation MSE anomaly averaged over the equatorial area (10°S–10°N, 90°E–110°E) during 10–20 May 2013. The middle panels are for 110°E–130°E, and the lower panels are for 130°E–150°E.

of insolation enhances the advection of MSE anomalies, allowing the MJO to propagate more smoothly. As a result, the absence of the diurnal cycle leads to stronger and more persistent MJO, as the advection processes are less countered by the retarding effects of LH, SH, and LW. The increased efficiency of MJO propagation in the NO_DC simulation highlights the critical role of the diurnal cycle in modulating these processes.

Table 3
Difference (NO_DC-CTL) in Fractional Contributions of the Individual MSE Budget Terms (No Units) to the Maintenance and Propagation of the MJO MSE Anomaly Averaged Over 10°S–10°N for Three Different Longitudinal Bands (90°E–110°E, 110°E–130°E, 130°E–150°E)

	dMSE/dt	HADV	VADV	LH	SH	LW	SW	R
Maintenance								
90°E–110°E	0.04	−0.06	−0.05	0.02	0.01	0.12	−0.05	0.01
110°E–130°E	0.10	−0.08	−0.15	0.05	0.05	0.11	0.01	0.11
130°E–150°E	0.05	−0.09	−0.06	0.06	0.01	0.08	0.03	0.02
Propagation								
90°E–110°E	0.27	0.07	0.07	0.03	0.02	0.06	−0.02	0.03
110°E–130°E	0.24	0.05	0.21	0.01	−0.04	−0.05	0.06	0.03
130°E–150°E	0.08	0.04	0.09	−0.05	−0.02	−0.04	0.08	0.02

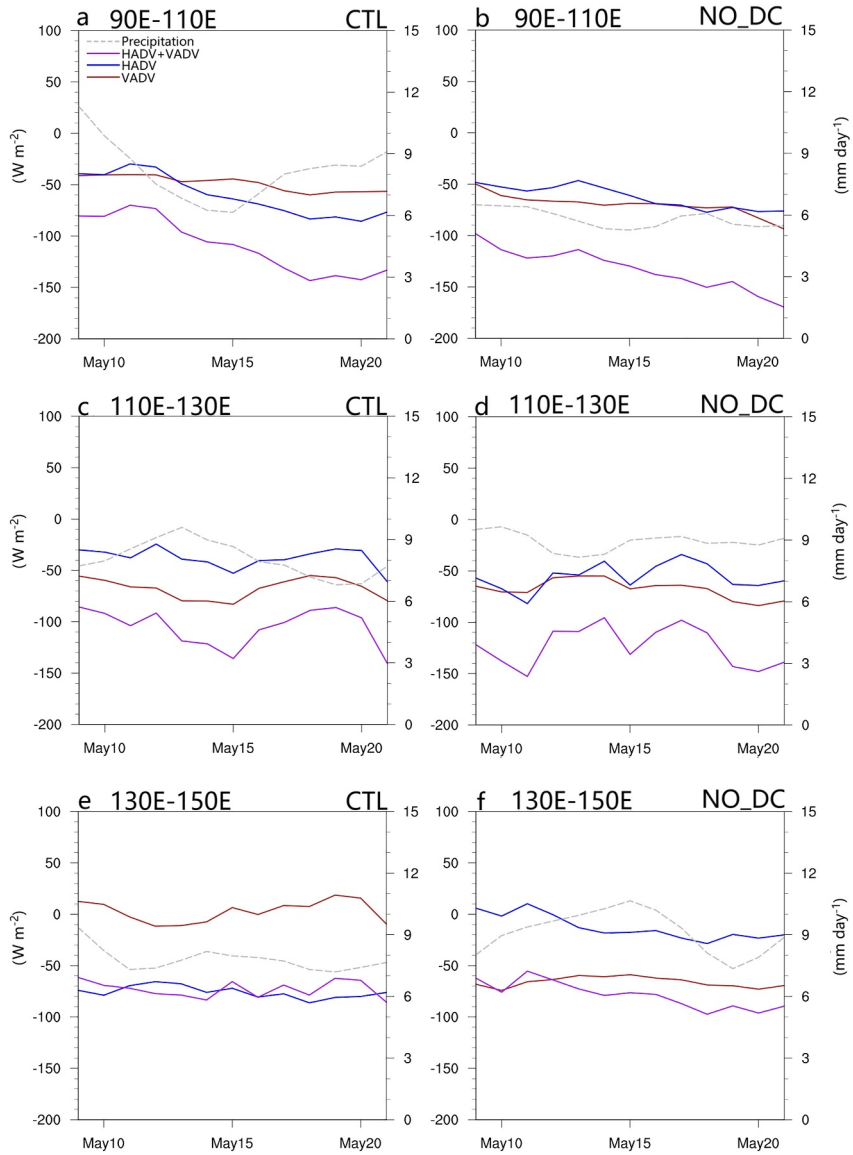

Figure 8. (Top panel) The 3-day running mean time series of the precipitation (black dashed line; mm day^{-1}; right *y*-axis) and advection terms (colored lines; W m^{-2}; left *y*-axis) from the (a) CTL, and (b) NO_DC simulations averaged over the equatorial area (10°S–10°N, 90°E–110°E) during 10–20 May 2013. The middle panels are for 110°E–130°E, and the lower panels are for 130°E–150°E.

Figure 8 shows the temporal evolution of precipitation and advection terms from both the CTL and NO_DC experiments. For MJO eastward propagation to occur, horizontal and VADV or other processes are required to supply moisture ahead of the convective center that must overcome the drying associated with suppressed surface fluxes within anomalous easterlies. In the CTL experiment (left panels), the net MSE advection (HADV + VADV) is generally less negative compared to the NO_DC run (right panels), particularly in the 90°E–110°E region (Figures 8a and 8b), where precipitation also shows a clearer peak around May 10th. This suggests that in the CTL run, there is less effective MSE transport to precondition the atmosphere ahead of the convection center, leading to weaker precipitation in the 110°E–130°E region (Figure 8c) and stalled propagation. In contrast, in the NO_DC simulation, the increased MSE advection (especially VADV) is sufficient to overcome the suppressed surface fluxes, supporting the eastward propagation of the MJO. In many models, the representation of the MJO is improved when the sensitivity of deep convection to free-tropospheric humidity is amplified, especially through the inhibition of convection under dry mid-tropospheric conditions. Ultimately, eastward-propagating

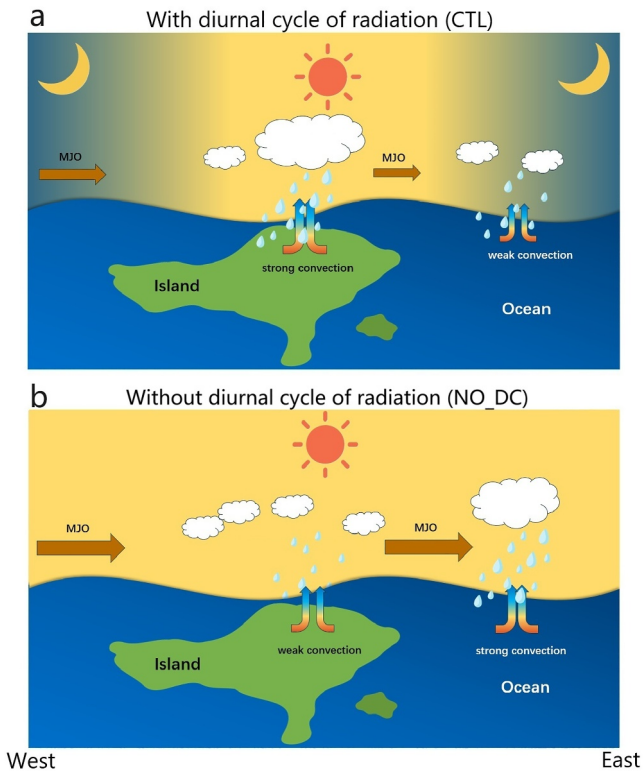

Figure 9. Schematic diagram showing the impact of (a) inclusion of diurnal cycle (CTL), and (b) the removal of diurnal cycle (NO_DC) on convection and propagation of Madden-Julian oscillation (MJO). The size of the MJO arrow indicates the strength of the MJO, while the cloud size represents the extent of convection or precipitation. The Maritime Continent (MC) barrier effect is more pronounced in CTL simulation with stronger convection over the islands, whereas convection shifts to the ocean in NO_DC simulation leading to persistent propagation of MJO across the MC.

moisture modes require a net MSE source that precedes convection. This supports the interpretation of the MJO as a moisture mode, wherein the balances between the sources and sinks of MSE govern both its amplification and propagation (Sobel & Maloney, 2013).

The CTL simulation, which includes the diurnal cycle, introduces variability in surface fluxes and radiative heating. This variability disrupts the advection-driven propagation of MSE anomalies by modulating land-sea breeze dynamics and convection patterns. Daytime convection over land competes with convection over the surrounding seas, creating a synchronized yet intermittent convective pattern across the MC. This competition hinders the eastward propagation of the MJO (Figure 9a), where enhanced land-based convection disrupts the continuity of convection over the seas. In contrast, the NO_DC simulation, which excludes the diurnal cycle, simplifies the MJO's trajectory. Without diurnal variability, convection shifts predominantly to the surrounding seas, resulting in 31.3% reduction in land precipitation and 25% increase in oceanic precipitation (Table 4). This dominance of oceanic convection supports a more robust and uninterrupted eastward propagation of the MJO (Figure 5b). The weakened land-sea breeze and reduced land-based convection in NO_DC lead to smoother vertical and HADV of MSE.

These findings underscore the importance of the diurnal cycle in modulating the MJO's interaction with the MC geography. By introducing variability in surface fluxes and convection, the diurnal cycle disrupts MJO propagation. This highlights the need to accurately represent the diurnal cycle in numerical models to improve predictions of MJO behavior and associated weather patterns.

4. Summary and Conclusion

We explored the impact of the diurnal cycle of insolation on an MJO event that weakened significantly while crossing the MC. Two simulations were performed: one that includes the natural diurnal cycle (CTL) and another eliminating it (NO_DC), whereby the incoming radiation at the TOA was held constant at its daily mean. In the CTL simulation, the diurnal cycle leads to competition between convection over the islands and the surrounding seas, driven by enhanced daytime convection over land that creates a synchronized pattern of convection over the entire MC. This weakens the MJO substantially as it moves across the MC, with heavy precipitation activity stalling over the islands. In contrast, the NO_DC simulation shows a more uninterrupted and robust eastward propagation of the MJO across the MC. The main results of our study are summarized as follows:

1. In the CTL simulation, strong land convection suppresses oceanic convection, creating a barrier to MJO propagation across the MC. In contrast, in the NO_DC simulation, the absence of diurnal cycle of insolation weakens the land-sea breeze, substantially reducing land convection and facilitating more continuous and persistent MJO propagation across the region (see schematic in Figure 9).
2. An analysis of the MSE budget reveals that differences in MSE between the CTL and NO_DC simulations are primarily driven by LE, particularly in the lower-to-mid troposphere, highlighting its central role in modulating MJO dynamics.
3. In both simulations, vertical and HADV of MSE act to disrupt MJO maintenance, whereas LW, LH, and SW contribute to its maintenance. The robust MJO maintenance in the NO_DC simulation is attributed to increased LW and reduced HADV and VADV. However, in the western MC (90°E–110°E), the reduction in SW in NO_DC compared to CTL opposes MJO maintenance.
4. In both simulations, vertical and HADV of MSE promote eastward MJO propagation, whereas LW and LH act to hinder it. In the NO_DC

Table 4
Precipitation (mm Day^{-1}) From CTL, NO_DC, and Their Differences (NO_DC Minus CTL) Over the Maritime Continent (10°S–10°N, 90°E–155°E) for 01–31 May 2013

Precipitation	CTL	NO_DC	NO_DC-CTL
All land	11.2	7.7	−3.5 (−31.3%)
All ocean	8.4	10.5	2.1 (25%)

simulation, the persistent eastward propagation of the MJO is attributed to increased HADV and VADV, along with reduced LW and LH. However, in the central MC (110°E–130°E), the increase in LH in NO_DC compared to CTL opposes MJO propagation.

Our study does not attempt to resolve the full range of complexities in the MC, such as fine-scale orographic effects, but instead focuses on isolating the role of the diurnal cycle of insolation in modulating MJO propagation. The WRF simulations at 10 km resolution adequately represent island-scale topographic features and associated land–sea breeze circulations, allowing us to assess the large-scale barrier effect on MJO propagation. While we acknowledge that finer-resolution simulations and targeted sensitivity tests would better resolve localized topographic trapping, such analyses are beyond the scope of this paper. Instead, our results should be viewed as complementary: by removing the diurnal cycle, we demonstrate how strong land-driven convection - amplified by topography - interacts with the large-scale MJO envelope, thereby shaping its propagation across the MC.

Furthermore, we employed an atmosphere-only regional model (WRF) without coupling to an interactive ocean, thereby enabling a direct assessment of how land-driven diurnal heating disrupts MJO propagation without the added complexity of air–sea feedbacks. This framework, which contrasts simulations with and without diurnal forcing, isolates the role of diurnal insolation in shaping MJO dynamics. When combined with a MSE budget analysis, this targeted design provides mechanistic insights into how diurnal processes disrupt or sustain MJO propagation, offering a complementary perspective to broader multi-model and coupled-system studies. In the future, we plan to incorporate an interactive ocean component to account for diurnal variations in SST and their feedback on surface fluxes and MJO evolution. A better understanding of these complex physical processes is essential for improving subseasonal-to-seasonal (S2S) predictions, not only over the MC but also globally, given the MJO's far-reaching influence on weather and climate systems.

In summary, this study advances our understanding of the MJO by leveraging an analysis of the MSE budget together with a novel LPT framework specifically designed to capture the eastward propagation of the MJO convective envelope. This methodological combination distinguishes our work from earlier studies that primarily relied on statistical composites or regional correlations to assess the role of the diurnal cycle. For example, Peatman et al. (2014) emphasized statistical modulation of MJO rainfall by the diurnal cycle over the MC, whereas our approach directly links the diurnal forcing to the large-scale MSE budget. Similarly, Hagos et al. (2016) highlighted the influence of diurnal land–sea breezes on MJO propagation, but here we quantify the energetic pathways through which such processes either sustain or hinder eastward propagation of convection. While Birch et al. (2016) and Lestari et al. (2022) discussed aspects of diurnal modulation using regional models, their analyses were confined to localized convection, whereas our tracking approach follows the evolving MJO envelope across the heterogeneous MC, thereby isolating spatial contrasts in the dominance of underlying processes.

Our findings reveal, likely for the first time, that the physical mechanisms governing MJO maintenance and propagation across the MC are not spatially uniform. The interplay between diurnal heating and land–sea contrasts exerts distinct, regionally varying impacts on MSE tendencies and convective organization. This demonstrates that the diurnal cycle does not impose a uniform influence on MJO, but rather a spatially varying one that critically shapes the MJO as it traverses the complex geography of the MC. These results provide new insights into why realistic simulations of the MJO remain particularly challenging for both regional and global models, and underscore the need to improve model representation of the diurnal cycle of convection in order to improve predictions of the MJO.

Conflict of Interest

The authors declare no conflicts of interest relevant to this study.

Data Availability Statement

WRF depository is available at https://github.com/wrf-model/WRF. The code to remove the diurnal cycle of insolation and related modules can be found in X. Zhou, (2025). Version 6.6.2 of the NCAR Command Language (NCL) used for making figures is developed openly at http://dx.doi.org/10.5065/D6WD3XH5. ERA5 (European Centre for Medium-Range Weather Forecasts Reanalysis v5) data are available from the Research Data Archive

at the National Center for Atmospheric Research, Computational and Information Systems Laboratory, at https://doi.org/10.5065/BH6N-5N20. The Tropical Rainfall Measuring Mission (TRMM) Version 7 3B42 and 3B43 Data Sets are available at https://disc.gsfc.nasa.gov/datasets?keywords=TRMM&page=1.

Acknowledgments
This work was supported by a Grant from the Climate Program Office (CPO) of the National Oceanic and Atmospheric Administration (NOAA, NA22OAR4310612) to Pallav Ray. Samson. M. Hagos's contribution was supported by the U.S. Department of Energy Office of Science Biological and Environmental Research as part of the RENEW Program. We would also like to acknowledge high-performance computing support from Cheyenne (doi: 10.5065/D6RX99HX) provided by NCAR's Computational and Information Systems Laboratory, sponsored by the National Science Foundation (NSF). The WRF model output code can be obtained from https://www2.mmm.ucar.edu/wrf/users/download/get_source.html. NCAR is sponsored by the NSF.

References

Abhik, S., Hendon, H. H., & Zhang, C. (2023). The Indo-Pacific maritime continent barrier effect on MJO prediction. *Journal of Climate*, *36*(3), 945–957. https://doi.org/10.1175/jcli-d-22-0010.1

Abhik, S., Zhang, C., & Hendon, H. H. (2023). The Indo-Pacific maritime continent barrier effect on MJO ensemble prediction. *Geophysical Research Letters*, *50*(21), e2023GL105462. https://doi.org/10.1029/2023gl105462

Ahn, M.-S., Kim, D., Kang, D., Lee, J., Sperber, K. R., Gleckler, P. J., et al. (2020). MJO propagation across the maritime continent: Are CMIP6 models better than CMIP5 models? *Geophysical Research Letters*, *47*(11), e2020GL087250. https://doi.org/10.1029/2020gl087250

Andersen, J. A., & Kuang, Z. (2012). Moist static energy budget of MJO-like disturbances in the atmosphere of a zonally symmetric aquaplanet. *Journal of Climate*, *25*(8), 2782–2804. https://doi.org/10.1175/jcli-d-11-00168.1

Bai, H., & Schumacher, C. (2022). Topographic influences on diurnally driven MJO rainfall over the maritime continent. *Journal of Geophysical Research: Atmospheres*, *127*(6), e2021JD035905. https://doi.org/10.1029/2021jd035905

Barrett, B. S., Densmore, C. R., Ray, P., & Sanabia, E. R. (2021). Active and weakening MJO events in the maritime continent. *Climate Dynamics*, *57*(1–2), 157–172. https://doi.org/10.1007/s00382-021-05699-8

Birch, C. E., Webster, S., Peatman, S. C., Parker, D. J., Matthews, A. J., Li, Y., & Hassim, M. E. (2016). Scale interactions between the MJO and the western Maritime continent. *Journal of Climate*, *29*(7), 2471–2492. https://doi.org/10.1175/jcli-d-15-0557.1

Chen, F., & Dudhia, J. (2001). Coupling an advanced land surface hydrology model with the Penn State–NCAR MM5 modeling system. Part I: Model implementation and sensitivity. *Monthly Weather Review*, *129*(4), 569–585. https://doi.org/10.1175/1520-0493(2001)129<0569:caalsh>2.0.co;2

Hagos, S. M., Zhang, C., Feng, Z., Burleyson, C. D., De Mott, C., Kerns, B., et al. (2016). The impact of the diurnal cycle on the propagation of Madden-Julian oscillation convection across the maritime continent. *Journal of Advances in Modeling Earth Systems*, *8*, 1552–1564. https://doi.org/10.1002/2016MS000725

Hersbach, H., Bell, B., Berrisford, P., Hirahara, S., Horányi, A., Muñoz-Sabater, J., et al. (2020). The ERA5 global reanalysis. *Quarterly Journal of the Royal Meteorological Society*, *146*(730), 1999–2049. https://doi.org/10.1002/qj.3803

Hong, S. Y., & Lim, J. O. J. (2006). The WRF single–moment 6–class microphysics scheme (WSM6). *Journal of Korean Meteorology Society*, *42*, 129–151.

Houze, R. A., Geotis, S. G., Marks, F. D., & West, A. K. (1981). Winter monsoon convection in the vicinity of North Borneo. Part I: Structure and time variation of the clouds and precipitation. *Monthly Weather Review*, *109*(8), 1595–1614. https://doi.org/10.1175/1520-0493(1981)109<1595:wmcitv>2.0.co;2

Hsu, H.-H., & Lee, M. Y. (2005). Topographic effects on the eastward propagation and initiation of the Madden–Julian oscillation. *Journal of Climate*, *18*(6), 795–809. https://doi.org/10.1175/jcli-3292.1

Iacono, M. J., Delamere, J. S., Mlawer, E. J., Shephard, M. W., Clough, S. A., & Collins, W. D. (2008). Radiative forcing by long–lived greenhouse gases: Calculations with the AER radiative transfer models. *Journal of Geophysical Research*, *113*(D13), D13103. https://doi.org/10.1029/2008jd009944

Ichikawa, H., & Yasunari, T. (2006). Time-space characteristics of diurnal rainfall over Borneo and surrounding oceans as observed by TRMM-PR. *Journal of Climate*, *19*(7), 1238–1260. https://doi.org/10.1175/jcli3714.1

Ichikawa, H., & Yasunari, T. (2008). Intraseasonal variability in diurnal rainfall over New Guinea and the surrounding oceans during austral summer. *Journal of Climate*, *21*(12), 2852–2868. https://doi.org/10.1175/2007jcli1784.1

Jiang, X. (2017). Key processes for the eastward propagation of the Madden-Julian oscillation based on multimodel simulations. *Journal of Geophysical Research: Atmospheres*, *122*(2), 755–770. https://doi.org/10.1002/2016jd025955

Jiang, X., Adames, Á. F., Kim, D., Maloney, E. D., Lin, H., Kim, H., et al. (2020). Fifty years of research on the Madden-Julian oscillation: Recent progress, challenges, and perspectives. *Journal of Geophysical Research: Atmospheres*, *125*(17), e2019JD030911. https://doi.org/10.1029/2019jd030911

Karlowska, E., Matthews, A. J., Webber, B. G. M., Graham, T., & Xavier, P. (2024). The effect of diurnal warming of sea-surface temperatures on the propagation speed of the Madden–Julian oscillation. *Quarterly Journal of the Royal Meteorological Society*, *150*(758), 334–354. https://doi.org/10.1002/qj.4599

Kerns, B. W., & Chen, S. S. (2016). Large-scale precipitation tracking and the MJO over the Maritime Continent and Indo-Pacific warm pool. *Journal of Geophysical Research: Atmospheres*, *121*(15), 8755–8776. https://doi.org/10.1002/2015jd024661

Kerns, B. W., & Chen, S. S. (2020). A 20-year climatology of Madden-Julian oscillation convection: Large-scale precipitation tracking from TRMM-GPM rainfall. *Journal of Geophysical Research: Atmospheres*, *125*(7), e2019JD032142. https://doi.org/10.1029/2019jd032142

Kiladis, G. N., Dias, J., Straub, K. H., Wheeler, M. C., Tulich, S. N., Kikuchi, K., et al. (2014). A comparison of OLR and circulation-based indices for tracking the MJO. *Monthly Weather Review*, *142*(5), 1697–1715. https://doi.org/10.1175/mwr-d-13-00301.1

Kim, D., Maloney, E. D., & Zhang, C. (2020). MJO propagation over the Maritime Continent. *The multiscale global monsoon system*, 261–272.

Kim, D., Sperber, K., Stern, W., Waliser, D., Kang, I. S., Maloney, E., et al. (2009). Application of MJO simulation diagnostics to climate models. *Journal of Climate*, *22*(23), 6413–6436. https://doi.org/10.1175/2009jcli3063.1

Kim, H., Ham, Y. G., Joo, Y. S., & Son, S. W. (2021). Deep learning for bias correction of MJO prediction. *Nature Communications*, *12*(1), 3087. https://doi.org/10.1038/s41467-021-23406-3

Kim, H. M., Kim, D., Vitart, F., Toma, V. E., Kug, J. S., & Webster, P. J. (2016). MJO propagation across the Maritime Continent in the ECMWF ensemble prediction system. *Journal of Climate*, *29*(11), 3973–3988. https://doi.org/10.1175/jcli-d-15-0862.1

Kim, J. K., & Sobel, A. H. (2014). Propagating versus nonpropagating Madden–Julian oscillation events. *Journal of Climate*, *27*(1), 111–125. https://doi.org/10.1175/jcli-d-13-00084.1

Lestari, S., King, A., Vincent, C., Protat, A., Karoly, D., & Mori, S. (2022). Variability of Jakarta rain-rate characteristics associated with the madden–julian oscillation and topography. *Monthly Weather Review*, *150*(8), 1953–1975. https://doi.org/10.1175/mwr-d-21-0112.1

Li, K., Yu, W., Yang, Y., Feng, L., Liu, S., & Li, L. (2020). Spring barrier to the MJO eastward propagation. *Geophysical Research Letters*, *47*(13), e2020GL087788. https://doi.org/10.1029/2020gl087788

Lim, K. S., & Hong, S. (2010). Development of an effective double-moment cloud microphysics scheme with prognostic cloud condensation nuclei (CCN) for weather and climate models. *Monthly Weather Review*, *138*(5), 1587–1612. https://doi.org/10.1175/2009mwr2968.1

Ling, J., Zhang, C., Joyce, R., Xie, P. P., & Chen, G. (2019). Possible role of the diurnal cycle in land convection in the barrier effect on the MJO by the Maritime Continent. *Geophysical Research Letters*, *46*(5), 3001–3011. https://doi.org/10.1029/2019gl081962

Liu, Z., Ostrenga, D., Teng, W., & Kempler, S. (2012). Tropical Rainfall measuring mission (TRMM) precipitation data and services for research and applications. *Bulletin of the American Meteorological Society*, *93*(9), 1317–1325. https://doi.org/10.1175/bams-d-11-00152.1

Love, B. S., Matthews, A. J., & Lister, G. M. (2011). The diurnal cycle of precipitation over the Maritime Continent in a high-resolution atmospheric model. *Quarterly Journal of the Royal Meteorological Society*, *137*(657), 934–947. https://doi.org/10.1002/qj.809

Lu, J., Li, T., & Wang, L. (2019). Precipitation diurnal cycle over the Maritime Continent modulated by the MJO. *Climate Dynamics*, *53*(9), 6489–6501. https://doi.org/10.1007/s00382-019-04941-8

Madden, R. A., & Julian, P. R. (1971). Detection of a 40–50 day oscillation in zonal wind in tropical Pacific. *Journal of the Atmospheric Sciences*, *28*(5), 702–708. https://doi.org/10.1175/1520-0469(1971)028<0702:doadoi>2.0.co;2

Matthews, A. J. (2000). Propagation mechanisms for the Madden-Julian oscillation. *Quarterly Journal of the Royal Meteorological Society*, *126*(569), 2637–2651. https://doi.org/10.1256/smsqj.56901

Mori, S., Jun-Ichi, H., Tauhid, Y. I., Yamanaka, M. D., Okamoto, N., Murata, F., et al. (2004). Diurnal land–sea rainfall peak migration over Sumatra Island, Indonesian Maritime Continent, observed by TRMM satellite and intensive rawinsonde soundings. *Monthly Weather Review*, *132*(8), 2021–2039. https://doi.org/10.1175/1520-0493(2004)132<2021:dlrpmo>2.0.co;2

Neena, J. M., Lee, J.-Y., Waliser, D., Wang, B., & Jiang, X. (2014). Predictability of the madden-julian oscillation in the intraseasonal variability hindcast experiment (ISVHE). *Journal of Climate*, *27*(12), 4531–4543. https://doi.org/10.1175/jcli-d-13-00624.1

Oh, J. H., Kim, B. M., Kim, K. Y., Song, H. J., & Lim, G. H. (2013). The impact of the diurnal cycle on the MJO over the Maritime Continent: A modeling study assimilating TRMM rain rate into global analysis. *Climate Dynamics*, *40*(3–4), 893–911. https://doi.org/10.1007/s00382-012-1419-8

Peatman, S. C., Matthews, A. J., & Stevens, D. P. (2014). Propagation of the Madden-Julian Oscillation through the Maritime Continent and scale interaction with the diurnal cycle of precipitation. *Quarterly Journal of the Royal Meteorological Society*, *140*(680), 814–825. https://doi.org/10.1002/qj.2161

Pohl, B., & Matthews, A. J. (2007). Observed changes in the lifetime and amplitude of the Madden-Julian Oscillation associated with interannual ENSO sea surface temperature anomalies. *Journal of Climate*, *20*(11), 2659–2674. https://doi.org/10.1175/jcli4230.1

Powers, J. G., Klemp, J. B., Skamarock, W. C., Davis, C. A., Dudhia, J., Gill, D. O., et al. (2017). The weather research and forecasting model: Overview, system efforts, and future directions. *Bulletin of the American Meteorological Society*, *98*(8), 1717–1737. https://doi.org/10.1175/bams-d-15-00308.1

Ramage, C. S. (1968). Role of a tropical "maritime continent" in the atmospheric circulation. *Monthly Weather Review*, *96*(6), 365–370. https://doi.org/10.1175/1520-0493(1968)096<0365:roatmc>2.0.co;2

Rauniyar, S. P., & Walsh, K. J. E. (2011). Scale interaction of the diurnal cycle of rainfall over the Maritime Continent and Australia: Influence of the MJO. *Journal of Climate*, *24*(2), 325–348. https://doi.org/10.1175/2010jcli3673.1

Ray, P., Zhang, C., Moncrieff, M. W., Dudhia, J., Caron, J. M., Leung, L. R., & Bruyere, C. (2011). Role of atmospheric mean state on the initiation of the Madden-Julian oscillation in a tropical channel model. *Climate Dynamics*, *36*(1–2), 161–184. https://doi.org/10.1007/s00382-010-0859-2

Ren, P., Kim, D., Ahn, M., Kang, D., & Ren, H. (2021). Intercomparison of MJO column moist static energy and water vapor budget among six modern reanalysis products. *Journal of Climate*, *34*(8), 2977–3001. https://doi.org/10.1175/jcli-d-20-0653.1

Rui, H., & Wang, B. (1990). Development characteristics and dynamic structure of tropical intraseasonal convection anomalies. *Journal of the Atmospheric Sciences*, *47*(3), 357–379. https://doi.org/10.1175/1520-0469(1990)047<0357:dcadso>2.0.co;2

Salby, M. L., & Hendon, H. H. (1994). Intraseasonal behavior of clouds, temperature and motion in the tropics. *Journal of the Atmospheric Sciences*, *51*(15), 2207–2224. https://doi.org/10.1175/1520-0469(1994)051<2207:ibocta>2.0.co;2

Savarin, A., & Chen, S. S. (2023). Land-locked convection as a barrier to MJO propagation across the Maritime Continent. *Journal of Advances in Modeling Earth Systems*, *15*(6), e2022MS003503. https://doi.org/10.1029/2022ms003503

Seo, K.-H., Wang, W., Gottschalck, J., Zhang, Q., Schemm, J.-K. E., Higgins, W. R., & Kumar, A. (2009). Evaluation of MJO forecast skill from several statistical and dynamical forecast models. *Journal of Climate*, *22*(9), 2372–2388. https://doi.org/10.1175/2008jcli2421.1

Sobel, A. H., & Maloney, E. D. (2013). Moisture modes and the eastward propagation of the MJO. *Journal of the Atmospheric Sciences*, *70*(1), 187–192. https://doi.org/10.1175/jas-d-12-0189.1

Sobel, A. H., Maloney, E. D., Bellon, G., & Frierson, D. M. (2010). Surface fluxes and tropical intraseasonal variability: A reassessment. *Journal of Advances in Modeling Earth Systems*, *2*(2). https://doi.org/10.3894/james.2010.2.2

Suzuki, T. (2009). Diurnal cycle of deep convection in super clusters embedded in the Madden-Julian oscillation. *Journal of Geophysical Research*, *114*(D22). https://doi.org/10.1029/2008jd011303

Tan, H., Ray, P., Barrett, B., Dudhia, J., & Moncrief, M. W. (2021). Systematic patterns in land precipitation due to convection in neighboring islands in the Maritime Continent during MJO propagation. *Journal of Geophysical Research: Atmospheres*, *126*(4), e2020JD033465. https://doi.org/10.1029/2020jd033465

Tan, H., Ray, P., Barrett, B., Dudhia, J., Moncrieff, M., Zhang, L., & Zermeno-Diaz, D. (2022). Understanding the role of topography on the diurnal cycle of precipitation in the Maritime Continent during MJO propagation. *Climate Dynamics*, *58*(11–12), 3003–3019. https://doi.org/10.1007/s00382-021-06085-0

Tan, H., Ray, P., Barrett, B., Tewai, M., Moncrieff, M. W., Zhang, L., & Zermeno-Diaz, D. (2020). Understanding the role of topography on the diurnal cycle of precipitation in the Maritime Continent during MJO propagation. *Climate Dynamics*, *58*(11–12), 3003–3019. https://doi.org/10.1007/s00382-021-06085-0

Tian, B., Waliser, D. E., & Fetzer, E. J. (2006). Modulation of the diurnal cycle of tropical deep convective clouds by the MJO. *Geophysical Research Letters*, *33*(20). https://doi.org/10.1029/2006gl027752

Tiedtke, M. (1989). A comprehensive mass flux scheme for cumulus parameterization in large-scale models. *Monthly Weather Review*, *117*(8), 1779–1800. https://doi.org/10.1175/1520-0493(1989)117<1779:acmfsf>2.0.co;2

Vitart, F., & Molteni, F. (2010). Simulation of the Madden–Julian oscillation and its teleconnections in the ECMWF forecast system. *Quarterly Journal of the Royal Meteorological Society*, *136*(649), 842–855. https://doi.org/10.1002/qj.623

Wang, S., Sobel, A. H., Tippett, M. K., & Vitart, F. (2019). Prediction and predictability of tropical intraseasonal convection: Seasonal dependence and the Maritime Continent prediction barrier. *Climate Dynamics*, *52*(9–10), 6015–6031. https://doi.org/10.1007/s00382-018-4492-9

Wei, Y., Pu, Z., & Zhang, C. (2020). Diurnal cycle of precipitation over the Maritime Continent under modulation of MJO: Perspectives from cloud-permitting scale simulations. *Journal of Geophysical Research: Atmospheres*, *125*(13), e2020JD032529. https://doi.org/10.1029/2020jd032529

Wheeler, M. C., & Hendon, H. H. (2004). An all-season real-time multivariate MJO index: Development of an index for monitoring and prediction. *Monthly Weather Review*, *132*(8), 1917–1932. https://doi.org/10.1175/1520-0493(2004)132<1917:aarmmi>2.0.co;2

Wolding, B. O., Maloney, E. D., & Branson, M. (2016). Vertically resolved weak temperature gradient analysis of the Madden-Julian oscillation in SP-CESM. *Journal of Advances in Modeling Earth Systems*, *8*, 1586–1619. https://doi.org/10.1002/2016MS000724

Yadav, P., & Straus, D. M. (2017). Circulation response to fast and slow MJO episodes. *Monthly Weather Review*, *145*(5), 1577–1596. https://doi.org/10.1175/mwr-d-16-0352.1

Yamanaka, M. D. (2016). Physical climatology of Indonesian Maritime Continent: An outline to comprehend observational studies. *Atmospheric Research*, *178*, 231–259. https://doi.org/10.1016/j.atmosres.2016.03.017

Yang, G. Y., & Slingo, J. (2001). The diurnal cycle in the tropics. *Monthly Weather Review*, *129*(4), 784–801. https://doi.org/10.1175/1520-0493(2001)129<0784:tdcitt>2.0.co;2

Zhang, C., & Hendon, H. H. (1997). Propagating and standing components of the intraseasonal oscillation in tropical convection. *Journal of the Atmospheric Sciences*, *54*(6), 741–752. https://doi.org/10.1175/1520-0469(1997)054<0741:pascot>2.0.co;2

Zhang, C., & Ling, J. (2017). Barrier effect of the Indo-Pacific Maritime Continent on the MJO: Perspectives from tracking MJO precipitation. *Journal of Climate*, *30*(9), 3439–3459. https://doi.org/10.1175/jcli-d-16-0614.1

Zhou, X. (2025). DC removal experiments. *Zenodo*. https://doi.org/10.5281/zenodo.14600529

Zhou, X., Wang, L., Hsu, P. C., Li, T., & Xiang, B. (2024). Understanding the factors controlling MJO prediction skill across events. *Journal of Climate*, *37*(20), 5323–5336. https://doi.org/10.1175/jcli-d-23-0635.1

Zhou, Y., Wang, S., & Fang, J. (2022). Diurnal cycle and dipolar pattern of precipitation over Borneo during an MJO event: Lee convergence and offshore propagation. *Journal of the Atmospheric Sciences*, *79*(8), 2145–2168. https://doi.org/10.1175/jas-d-21-0258.1

Zhou, Y., Wang, S., & Fang, J. (2023). Diurnal cycle and dipolar pattern of precipitation over Borneo during the MJO: Linear theory and nonlinear sensitivity experiments. *Journal of Geophysical Research: Atmospheres*, *128*(5), e2022JD037616. https://doi.org/10.1029/2022jd037616